Spatial and spectral properties of the high-order harmonic emission in argon for seeding applications

Xinkui He,[1] M. Miranda,[1,*] J. Schwenke,[1,2] O. Guilbaud,[1,†] T. Ruchon,[1,‡] C. Heyl,[1] E. Georgadiou,[1] R. Rakowski,[1] A. Persson,[1] M. B. Gaarde,[3] and A. L'Huillier[1]

[1]*Department of Physics, Lund University, P.O. Box 118, SE-221 00 Lund, Sweden*

[2]*Max-lab, Lund University, P.O. Box 118, SE-221 00 Lund, Sweden*

[3]*Department of Physics and Astronomy, Louisiana State University, Baton Rouge, Los Angeles 70803-4001, USA*

(Received 24 November 2008; published 22 June 2009)

We characterize and control the harmonic emission in the spectral and spatial domains in order to define in which conditions the harmonic radiation can be a high-quality seed for soft x-ray and x-ray free-electron lasers. The length of the gas cell, where harmonics are generated, was optimized and the energy per pulse was determined in absolute value with a calibrated x-ray photodiode. The beam spatial profile was measured and, in some conditions, a very collimated beam with a half-angle divergence below 1 mrad could be obtained. We also show that increasing the intensity of the fundamental laser field leads to a considerable broadening of the bandwidth of the harmonic radiation, allowing us to cover a large spectral range. This effect is due to fundamental reshaping leading to an efficient phase matching of both short- and long-trajectory contributions.

DOI: 10.1103/PhysRevA.79.063829 PACS number(s): 42.65.Ky, 32.80.Rm, 32.80.Qk

I. INTRODUCTION

A lot of effort is devoted world wide to the development of coherent light sources in the extreme ultraviolet (xuv) range with laserlike properties. Different paths are being explored, from x-ray free-electron lasers (XFELs), based on the self-amplification of the synchrotron radiation emitted by relativistic electron bunches [1] to soft x-ray lasers (SXRLs), relying on the realization of a population inversion in highly charged ions obtained in a hot dense plasma [2]. These two approaches lead to high-energy xuv pulses with, in general, poor coherence properties compared to conventional lasers since the xuv beams result from the direct amplification of the spontaneous emission emitted at one extremity of the medium. High-order harmonics emitted during the nonlinear interaction between an intense ultrashort laser and a gas [3,4] inherit most of the desirable properties of the driving laser in terms of the spatial and temporal coherence but suffer from low conversion efficiencies, resulting in pulse energies typically in the nJ range [5]. A straightforward idea explored in several laboratories around the world [6–8] is to use harmonic radiation to seed the first mentioned sources, thus combining the coherence and flexibility of the harmonics with the high output energy of XFELs or SXRLs.

Seeding requires well-characterized and optimized harmonics. The spatial wave front and spectral content should be of high quality and the energy per unit of bandwidth as high as possible to overcome the spontaneous emission in the amplifier. Many studies have been devoted to characterize the harmonic spectra [9,10] or the spatial profile [11,12] of high-order harmonics, however, often separately. In addition, the harmonic frequency should be matched to a given x-ray plasma spectral line. Previous work uses a high-intensity frequency-chirped fundamental field to spectrally modulate and, to some extent, tune the high-energy part of the high-order harmonic generation spectrum [13,14]. An adaptive spectral filter (DAZZLER) has also been used to provide some tunability of the high-harmonic spectrum [15].

In the present paper, we discuss the characteristics of the harmonic radiation generated in argon around 30 nm by a rather high-energy laser driver with about 100 mJ per pulse in 40 fs at 800 nm wavelength. The spectrum, spatial profile, and energy per pulse are determined and optimized for different focusing geometries and medium lengths. We also show that the spectral bandwidth is considerably increased by simply using a higher laser intensity. We concentrate on the wavelength range between 20 and 40 nm, which can be reached using Ar as generating gas. In Sec. II, we describe the main physics of harmonic generation useful for this work. In Sec. III, we present the experimental method and results.

II. BRIEF SUMMARY OF THE PHYSICS OF HIGH-ORDER HARMONIC GENERATION

A. Single-atom response

The physical origin of harmonic generation can be easily understood by a simple semiclassical picture [16,17]. When an atom is exposed to an intense infrared laser field, the atomic potential is considerably distorted by the strong electric field. An electron from the outer shell may tunnel through the Coulomb barrier and ionize. This electron is then accelerated by the laser field, driven back to the parent ion when the direction of the electric field changes sign, and may recombine to the ground state, thereby emitting a high-energy photon. This energy is equal to the atomic ionization energy (I_p) plus the energy acquired during the acceleration.

*Also at IFIMUP/IN, Department of Physics, University of Porto, Portugal.

†Also at LIXAM, CNRS, Univ Paris-Sud, UMR n 8624, Orsay F-91405, France.

‡Also at CEA-Saclay, DSM, Service des Photons, Atomes et Molécules, 91191, Gif-sur-Yvette, France.

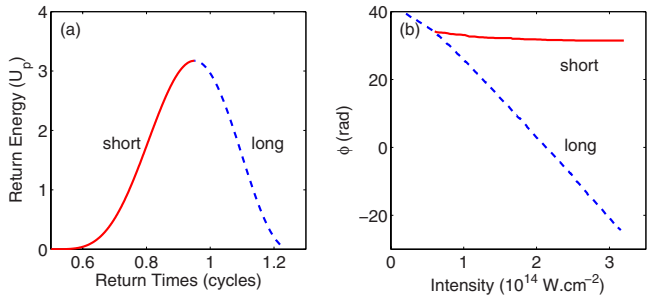

FIG. 1. (Color online) (a) Classical calculation of the kinetic energy of the electron as a function of the return time. (b) Calculation of the intensity dependence of the 19th harmonic phase for the short and long trajectories using the strong-field approximation [19].

This process occurs every half cycle of the driving laser, so that the emitted radiation is periodic with a periodicity equal to 1.3 fs, for a 800 nm fundamental laser field. The spectrum consists of harmonic peaks at odd multiples of the incident frequency. The kinetic energy (E_c) acquired during the electron excursion in the continuum can be calculated using a simple classical calculation, which provides to the experimentalist a useful guide to estimate the available spectral range (W) according to the formula $W=I_p+E_c$. Results of such calculations are presented in Fig. 1(a). The kinetic energy gained is plotted in units of the ponderomotive energy U_p related to the laser field amplitude (E) by $U_p=e^2E^2/4m\omega^2$ where e and m are the charge and mass of electron and ω laser frequencies. U_p (expressed in eV) can also been written as $9.34\lambda^2 I$ where the laser wavelength λ is in μm and the laser intensity I is in 10^{14} W/cm^2 units. For example, for $\lambda=0.8$ μm, $I=2\times10^{14}$ W/cm^2, the maximum kinetic energy is 38 eV, and the maximum photon energy generated in Ar is about 54 eV. The abscissa in Fig. 1(a) indicates the return time of the electron in units of the laser cycle (2.7 fs). This figure shows that there are two possible electron trajectories leading to the same return energy below the maximum energy. The trajectory with the longer excursion time is called the long trajectory, while that with the shorter excursion time is called short.

The phase accumulated by the electron on these trajectories is transferred to the emitted radiation field. The phase of the harmonic light is therefore not simply related to the phase of the driving laser but also includes an intrinsic phase component that can vary rapidly with laser intensity. This intrinsic phase, which is weakly dependent on the process order, has consequences for both spatial and spectral emission characteristics, and we indicate in Fig. 1(b) its variation with the intensity for the 19th harmonic generated in Ar calculated using the strong-field approximation [18,19]. The two branches refer to the short (red) and long (blue) trajectories. For $I>10^{14}$ W/cm^2, in the so-called plateau region, the intrinsic phase can be approximated by $\Phi_j(\mathbf{r},t)=\alpha_j I(\mathbf{r},t)$, where j refers to the trajectory (short or long). The harmonic field is the coherent sum of two contributions,

$$E_h(\mathbf{r},t)=\sum_{s,l} A_{hj}(\mathbf{r},t)e^{i\omega_h t-i\alpha_j I(\mathbf{r},t)}, \tag{1}$$

where A_{hj} denotes the amplitude of the contribution of the trajectory j to the harmonic field with frequency ω_h. We also indicate in Table I the values of these α coefficients for the short and long trajectories, for a few harmonics discussed in the present work [19]. Assuming a Gaussian distribution for the fundamental and harmonic fields, both in space and time, we can estimate the divergence and spectral bandwidth of the harmonic field according to

$$\theta_j=\frac{\lambda_h}{\pi w_h}\sqrt{1+4\alpha_j^2 I_0^2\frac{w_h^4}{w_f^4}}, \tag{2}$$

and

$$\Delta\lambda_j=\frac{\lambda_h^2}{\pi c\tau_h}\sqrt{1+4\alpha_j^2 I_0^2\frac{\tau_h^4}{\tau_f^4}}. \tag{3}$$

λ_h, w_h, and τ_h denote the wavelength, beam waist, and pulse width of the harmonic field and w_f, τ_f, and I_0 are the beam waist, pulse width, and peak intensity of the fundamental field. If the second terms in the roots are negligible, the harmonic field is Fourier transform limited in the time domain and diffraction limited in space. In general, phase effects lead to the deviation from the Fourier limit, especially for high intensities and long trajectories. Upper values for $\theta_j(j=s,l)$ and $\Delta\lambda_j$ are given in Table I using $w_f=150$ μm, $\tau_f=40$ fs, and $I_0=1.5\times10^{14}$ W/cm^2, representing typical experimental values and assuming $w_h/w_f=\tau_h/\tau_f=1$. In reality, these ratios are slightly below one and decrease with the process order since high-order harmonics require higher laser intensity to be generated and are emitted over a smaller diameter and shorter pulse duration. The values indicated in Table I might

TABLE I. Useful parameters for the 19th to the 31st harmonics in Ar. The intensity of the laser field used for the calculation is 1.5×10^{14} W/cm^2 and the unit for α is 10^{-14} W^{-1} cm^2.

Order	19	21	23	25	27	29	31
λ_h (nm)	42.1	38.1	34.8	32.0	29.6	27.6	25.8
α_s	−1.0	−1.8	−2.7	−3.8	−5.1	−6.9	−9.8
α_l	−22.9	−22.2	−21.5	−20.5	−19.2	−17.5	−14.8
θ_s (mrad)	0.3	0.4	0.6	0.8	1.0	1.2	1.6
θ_l (mrad)	6.1	5.4	4.8	4.2	3.6	3.1	2.4
$\Delta\lambda_s$ (nm)	0.2	0.2	0.2	0.3	0.4	0.5	0.5
$\Delta\lambda_l$ (nm)	3.2	2.6	2.1	1.7	1.4	1.0	0.8

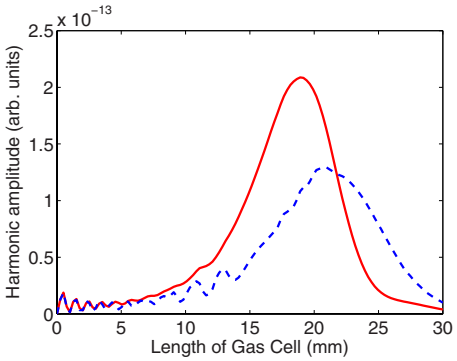

FIG. 2. (Color online) Phase matching contribution to the harmonic intensity as a function of cell length for short (red solid) and long (blue dashed) trajectories.

be used as a guide to estimate upper values for the spatial and spectral widths of the HHG radiation.

B. Propagation

The optimization of the harmonic emission requires not only a strong single-atom response but also that all of the atoms in the medium emitted in phase. For the sake of simplicity, we here give a simple description of propagation using a one-dimensional approximation, along the propagation axis (z). More advanced calculations accounting also for off-axis effects will be presented in Sec. III. Phase matching is realized when the variation in the difference between the phase of the qth harmonic field generated in the medium and that of the polarization driving it, equal to

$$\delta\Phi_q(z,t) = \int \Delta k_q(z',t)dz' + q \arctan(z/z_R) + \alpha_j I(z,t), \tag{4}$$

is minimized over the medium length [20]. In the right-hand side of Eq. (4), the first term denotes the influence of dispersion, which includes two opposite contributions, from the neutral medium and the free electrons. The second term indicates the influence of focusing (z_R denoting the Rayleigh length of the fundamental beam). Finally, the third term is the single-atom phase described above, which strongly depends on the trajectory. For loose focusing geometries, in general, the contribution of dispersion effects is stronger than the geometrical and single-atom phase variations, both for a neutral medium and for a strongly ionized medium. The first condition to achieve phase matching is to (approximately) cancel the neutral atom and free-electron dispersion, which is achieved for a degree of ionization of the medium of approximately 7% in argon. The phase variation due to the geometrical phase and to the single-atom phase (especially in the case of the long trajectory) needs to be included for a correct description of phase matching [21,22]. In addition, the absorption in general limits the conversion efficiency [23].

Figure 2 shows the results of calculations performed for the 21st harmonic in argon using a one-dimensional model described in [24], including all of the phase terms in Eq. (4),

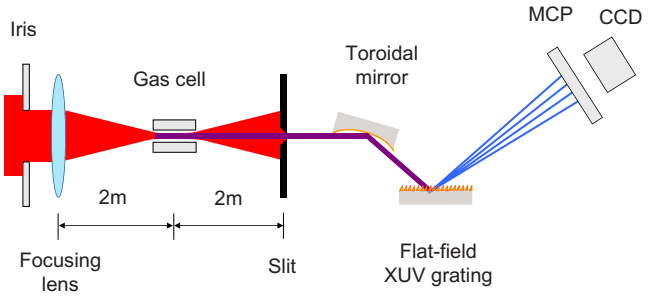

FIG. 3. (Color online) Experimental setup.

and consisting in summing all of the microscopic contributions over a certain length. The red and blue curves refer to the contribution of the short and long trajectories considered separately in the calculation, with the same single-atom response amplitude. The oscillations observed for short length media indicate that phase matching is not realized and that the field generated at some location in the medium is canceled by that generated in another location. The quadratic increase from $L=12$ mm is characteristic of phase matching. The harmonic yield saturates and eventually decreases when the absorption limit is reached. The phase variation for the long-trajectory contribution leads to a shift in the optimal medium length. The curves shown in Fig. 2 depend only weakly on the process order; for example, the short trajectory contribution of the 15th (respectively, 25th) harmonic is maximized for $L=16$ mm (respectively, $L=20$ mm). These results obtained with a one-dimensional model might change a little when generalizing to three dimensions, when considering other laser intensities and gas pressures. Our aim here was to illustrate the physics of phase matching of high-order harmonics rather than simulate a realistic experimental situation.

The conclusion of our model is that efficient, absorption-limited, and phase matching of high-order harmonics may be achieved by using sufficiently long media. Another way would be to have a cell with a length corresponding to the absorption length (or equal to a few times the absorption length) and to locate it at the position where the intensity is such that phase matching can be achieved. Experimentally, the first solution is much easier. Other effects, such as a spatiotemporal modification of the fundamental field [25], leading in particular to defocusing, could also favor phase matching of high-order harmonic generation in long media [26] (see also the discussion below).

III. EXPERIMENTAL METHOD AND RESULTS

A. Measurement of spatial and spectral profiles

Our experimental setup is shown in Fig. 3. The laser is an amplified Ti:sapphire 10 Hz system delivering 40 fs pulses around 800 nm with an energy up to 1 J. The results presented below are obtained with only a fraction of this energy less than 100 mJ. Furthermore, the 50-mm-diameter beam is apertured down by an iris with variable diameter (with a diameter typically between 11 and 16 mm), so that only about a few mJ infrared energy is actually sent into our ex-

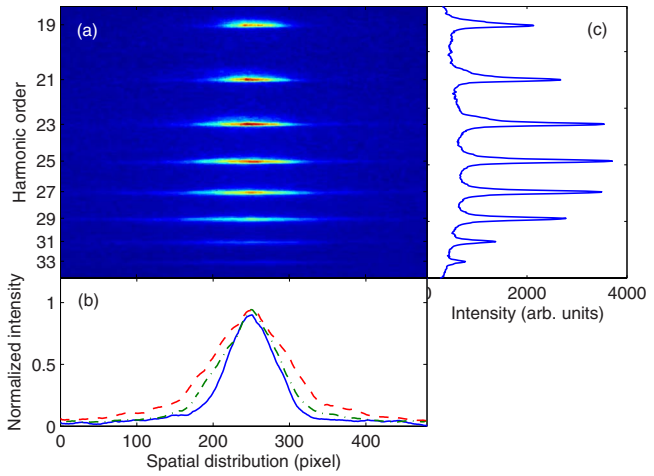

FIG. 4. (Color online) (a) Experimental measurement using a 21 mm Ar gas cell and a fundamental intensity of $I=10^{14}$ W/cm^2; (b) spatial profile of the 19th (blue solid), 23rd (green dash dotted), and 27th (red dashed) harmonic. (c) Spatially integrated spectrum.

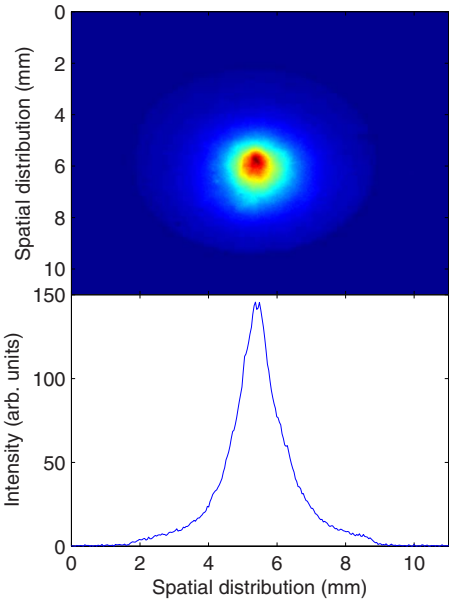

FIG. 5. (Color online) Spatial profile of the total harmonic yield transmitted through the Al filter measured at 2 m from the 15 mm gas cell. The infrared beam was focused just at the beginning of the cell. The aperture was 14 mm.

perimental setup. The beam is focused by a lens with 2 m focal length into a gas cell with 1 mm transverse diameter and variable length (from 3 to 20 mm). The harmonic spectra are detected by a flat-field xuv spectrometer, with a 100 μm entrance slit, located at approximately 2 m from the gas jet. An xuv microchannel plate (MCP) combined with a charge-coupled device camera is used to capture the final image. In contrast to many previous measurements [11,12], we do not image the harmonic source but a slice of its profile at a relatively long distance (2 m) from the source, which gives us the possibility to measure the spatial profile in the far field (and therefore the divergence) of the beam [27,28]. Our spectral resolution is estimated to be 0.2 nm.

A typical experimental spectrum is shown in Fig. 4. Harmonics are shown from the 19th to the 33rd, corresponding to a spectral range of 42–24 nm or in energy 29–51 eV. Spatial profiles are shown in the horizontal direction, while the vertical one shows spectra. Figure 4(b) shows some spatial profiles, while the spatially-integrated spectrum is presented in (c). These measurements show evidence for contributions from the short trajectory, leading to a narrow collimated beam and also from the (weaker) long trajectory, with much higher divergence. In the cut-off region, both contributions merge together.

In order to avoid any influence of the spectrometer collecting optics on the harmonic spatial profile, we have measured it directly by taking an image with the MCP at about 2 m from the gas cell. The fundamental field and the low-order harmonics (up to the 11th) were removed by an absorption in a 200-nm-thin Al filter. A typical result is shown in Fig. 5. A relatively narrow peak is superposed on a broad pedestal, which can be attributed to the main two quantum paths responsible for harmonic generation. The harmonic beam diameter could be measured by comparing with the diameter of the aperture on which the filter was mounted and which could be observed on the MCP. The full width at half maximum is 1.4 mm and the corresponding beam divergence is 0.7 mrad. This agrees with the predictions presented above (Table I) for the (dominant) short trajectory and for the strong 23rd–25th harmonics. The ratio between the short- and long-trajectory contributions is affected by the position of the focus of the infrared beam in the gas cell. In agreement with previous work [21], we find that the short trajectory is enhanced compared to the long one when the focus position is before the gas cell.

B. Measurement of the harmonic pulse energy

The pulse energy of the high-order harmonic radiation was measured by using a calibrated xuv photodiode, with good sensitivity from 1 eV to 6 keV. The diode could be moved under vacuum before the flat-field xuv spectrometer, so that we could measure the energy and the corresponding spectrum within the same series of measurements. Two 200 nm Al filters were needed to block the fundamental beam. The number of the electrons N_e generated from the photodiode is the integral of the measured current. The number of the photons at each harmonic frequency is obtained through the equation

$$N_e = \sum_q \eta_q t_q N_q, \tag{5}$$

where N_q denotes the number of photons generated at the qth harmonic frequency, t_q is the transmission by the Al filters and η_q is the quantum efficiency of the photodiode for the qth harmonic. The absorption from the Al filters can be estimated by calculating the transmission function of Al, accounting for the effect of a thin layer of oxide, which unfortunately reduces the transmission and introduces an uncertainty in the energy determination. Figure 6 shows the transmission of 200 nm Al (blue line), as well as that of 200 nm Al, plus 20 nm oxide (10 nm on each side), which is a

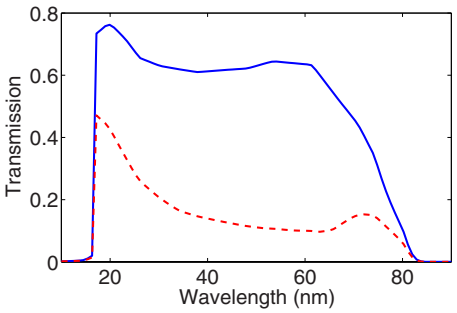

FIG. 6. (Color online) Calculated transmission function for 200 nm Al filter (blue solid) and with 10 nm oxidation layer on each side (red dashed).

rough estimation of the oxide layer on the filters used in this experiment [29]. From the relative ratios between the generated harmonics obtained from spectral measurements, the number of photons per harmonic, the pulse energy, as well as the conversion efficiency can be deduced. Results of measurements performed in optimized conditions [with a 19-mm-length gas cell (see below)] are presented in Table II.

C. Optimization of the output energy by varying the cell length

Figure 7(a) shows the variation in the harmonic energy as a function of cell length for a few harmonics. The focus was located at the center of the cell. The saturation effect observed is attributed to absorption, which is more important for the low-order harmonics than for the high-order ones. Figure 7(b) shows the 23rd harmonic spatial profile obtained at $\sim 2\times 10^{14}$ W/cm^2, with gas cells of different lengths and an aperture before the lens equal to 13 mm. The central part of the angular profile, which reflects the contribution from the short trajectory, is approximately constant with order and with cell length, on the order of 1 mrad.

Increasing the cell length results in an increased harmonic energy as well as the appearance of the long-trajectory contribution, with higher divergence. The predictions of our model (see Fig. 2) agree quite well with the experimental observation, showing a saturation for medium lengths of 20 mm and an increase in the contribution of the long trajectory as the length increases. The latter effect is of interest for seeding applications since the contribution of the long trajectory can be made spectrally broader at high laser intensity, thus, providing increased possibility to match the gain profile of an amplifier, as explained below.

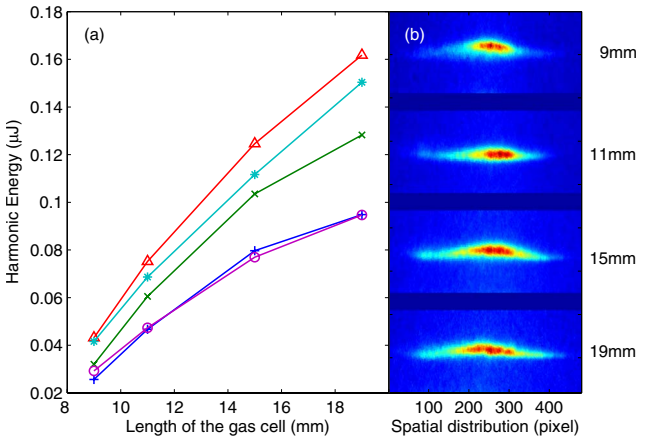

FIG. 7. (Color online) (a) Harmonic energy as a function of cell length for the 13th (line with plus), 17th (line with x mark), 21st (line with triangle), 23rd (line with star), and 27th (line with circle) order. (b) Spatial distribution of 23rd harmonic for different gas cell lengths.

D. Increasing the spectral range between consecutive harmonics

Spectra obtained from two different fundamental energies by changing iris diameters are shown in Fig. 8. The harmonic spectra get broadened as the input energy increases more than the prediction of Eq. (3) for a single trajectory. In addition, interference structures appear. This complicated structure appears in connection with an ionization-induced spatiotemporal reshaping of the laser beam, which improves the phase matching conditions for the long trajectory. The short trajectory is well phase matched both before and after the reshaping, and we therefore see spectral interference between the contributions from both trajectories [30]. Similar structures have been observed in previous work [27,28] and interpreted in terms of interference between the contribution of the two (short and long) trajectories, without—however—explaining the reason for both contributions to be of the same strength.

Our interpretation is supported by theoretical calculations including both the microscopic and macroscopic responses of the argon gas to the intense laser pulse. The results were calculated via the coupled nonadiabatic solutions of the time-dependent Schrödinger equation, within the strong-field approximation [17], and the Maxwell wave equation. Our approach is described in detail in [20]. As initial conditions for the calculation, we use similar parameters as the experiment, in terms of peak intensity, duration, and focusing conditions for the laser beam, and density and length of the argon cell.

TABLE II. Optimized high-order harmonic energy and conversion efficiency.

Harmonic order	17	19	21	23	25	27
Transmission	0.12	0.13	0.15	0.16	0.19	0.21
Photon number ($\times 10^{10}$)	3.03	2.98	3.10	2.63	1.60	1.41
Energy (μJ)	0.13	0.14	0.16	0.15	0.10	0.09
Efficiency ($\times 10^{-6}$)	6.8	7.5	8.6	8.0	5.3	5.0

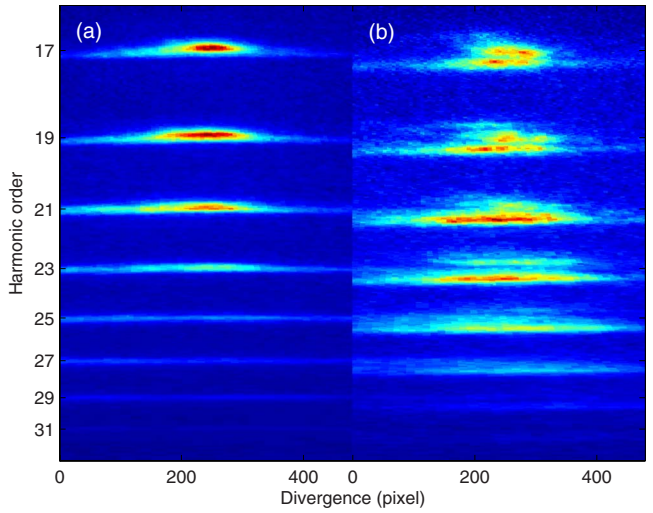

FIG. 8. (Color online) Harmonic spectra at two different intensities measured to be (a) 2×10^{14} W/cm^2 and (b) $\sim5\times10^{14}$ W/cm^2. A 21 mm gas cell was used and the focus point of the infrared beam was in the middle of the cell. Note the significant blue shift of the spectral distribution at high intensity.

The calculated far-field spatiospectral profiles of harmonics 17–21 are shown in Figs. 9(a) and 9(b). At low intensity, the very loose focusing conditions strongly favor phase matching of the short trajectory, and the resulting harmonics are spectrally narrow and well behaved. The contribution from the long trajectory in these conditions can barely be seen in Fig. 9(a) as a faint halo around the 19th harmonic,

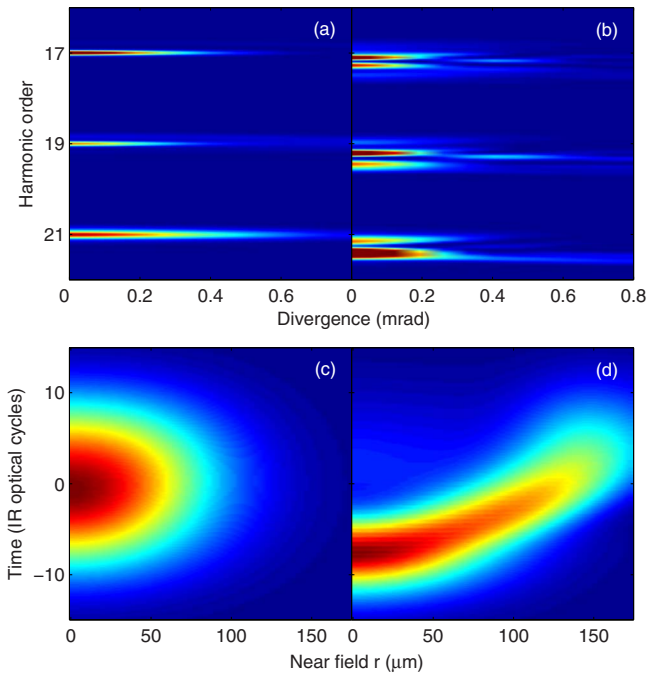

FIG. 9. (Color online) Calculated far-field spatial profile of different harmonic for two different peak intensities (a) 1×10^{14} W/cm^2 and (b) 3.3×10^{14} W/cm^2. Spatiotemporal distribution of corresponding fundamental beam at the exit of the medium (c) and (d).

most prominent on the low-frequency side and at divergences above 0.6 mrad. At high intensity, the harmonic spectra are much broader, exhibit interference fringes, and are blueshifted relative to the low-intensity case. As mentioned above, the interference is the result of both short- and long-trajectory contributions being well phase matched by the strongly reshaped laser beam. Figures 9(c) and 9(d) show the spatiotemporal profile of the laser beam in the near field, at the end of the argon medium. The high-intensity beam has undergone violent spatiotemporal reshaping which results in defocusing, strong blueshifting on axis, and the overall change in shape where the laser envelope reaches its maximum at different times for different radii. The reshaping happens after a few mm of propagation and then does not change much through the remainder of the medium. In the calculations, we see a strong increase in the long-trajectory contribution around the propagation distances where the reshaping sets in, with a significant component on axis. The short- and long-trajectory contributions thus interfere in the far field, leading to the two or three horizontal stripes observed in Figs. 9(b) and 8(b).

This effect provides an easy way for covering a larger spectral range, which is very important for seeding x-ray laser plasmas. For example, the 25th harmonic (32 nm) is close to the x-ray lasing lines of 31.2 nm (Ne-like Sc), 32.6 nm (Ne-like Ti), and 32.8 nm (Ni-like Kr) and can be broadened to reach these lines simply by increasing the laser intensity. It has been suggested previously [13,14] that harmonics could be tuned by changing the chirp of the fundamental field. In such an experiment, several parameters are varied at the same time: chirp, pulse duration, and laser intensity. We believe that the main effect is due to the variation in the laser intensity. In addition, the fundamental chirp may induce additional or reduced spectral broadening depending on the sign of the chirp.

IV. CONCLUSION

In this work, we have studied the spectral and spatial properties of high-order harmonics generated in argon gas. The absolute value of the energy emitted per harmonic pulse was estimated in optimized conditions. We found that the use of long gas cells (20 mm) led to higher energies and more collimated xuv beams. Large spectral bandwidths, close to the interval between consecutive harmonics, could be achieved by increasing the intensity of the infrared beam in the gas cell leading to an improved phase matching of the long trajectory.

ACKNOWLEDGMENTS

This research was supported by the European Union project NEST-ADVENTURE under Grant No. 012843-2 TUIXS, the Marie Curie actions EST MAXLAS, IIF OHIO, and EIF Attotech, the Knut and Alice Wallenberg Foundation, the Swedish Science Council, and the U.S. National Science Foundation through Grant No. PHY-044923. We thank B. Schütte, T. Eberle, J. Klemmer, F. Geier, and E. Pourtal, for their help in some early stage of this experiment.

[1] J. Feldhaus, J. Arthur, and J. B. Hastings, J. Phys. B **38**, S799 (2005).
[2] D. L. Matthews *et al.*, Phys. Rev. Lett. **54**, 110 (1985).
[3] A. McPherson *et al.*, J. Opt. Soc. Am. B **4**, 595 (1987).
[4] M. Ferray *et al.*, J. Phys. B **21**, L31 (1988).
[5] Harmonic energies per pulse on the order of a μJ have been reached by several groups; see, for example, J.-F. Hergott *et al.*, Phys. Rev. **66**, 021801 (2002); E. Takahashi *et al.*, J. Opt. Soc. Am. **20**, 158 (2003).
[6] P. Zeitoun *et al.*, Nature (London) **431**, 426 (2004).
[7] Y. Wang *et al.*, Nat. Photonics **2**, 94 (2008).
[8] G. Lambert *et al.*, Nat. Phys. **4**, 296 (2008).
[9] L. Nugent-Glandorf, M. Scheer, M. Krishnamurthy, J. W. Odom, and S. R. Leone, Phys. Rev. A **62**, 023812 (2000).
[10] H. T. Kim *et al.*, J. Phys. B **37**, 1141 (2004).
[11] J. W. G. Tisch, R. A. Smith, J. E. Muffett, M. Ciarrocca, J. P. Marangos, and M. H. R. Hutchinson, Phys. Rev. A **49**, R28 (1994).
[12] P. Salières *et al.*, J. Phys. B **27**, L217 (1994).
[13] H. T. Kim, D. G. Lee, K. H. Hong, J. H. Kim, I. W. Choi, and C. H. Nam, Phys. Rev. A **67**, 051801(R) (2003).
[14] Z. Chang, A. Rundquist, H. Wang, I. Christov, H. C. Kapteyn, and M. M. Murnane, Phys. Rev. A **58**, R30 (1998).
[15] D. H. Reitze *et al.*, Opt. Lett. **29**, 86 (2004).
[16] P. B. Corkum, Phys. Rev. Lett. **71**, 1994 (1993).
[17] M. Lewenstein, P. Balcou, M. Y. Ivanov, A. L'Huillier, and P. B. Corkum, Phys. Rev. A **49**, 2117 (1994).
[18] M. Lewenstein, P. Salieres, and A. L'Huillier, Phys. Rev. A **52**, 4747 (1995).
[19] K. Varju *et al.*, J. Mod. Opt. **52**, 379 (2005).
[20] M. B. Gaarde, J. L. Tate, and K. J. Schafer, J. Phys. B **41**, 132001 (2008).
[21] P. Salières, A. L'Huillier, and M. Lewenstein, Phys. Rev. Lett. **74**, 3776 (1995).
[22] F. Lindner, W. Stremme, M. G. Schatzel, F. Grasbon, G. G. Paulus, H. Walther, R. Hartmann, and L. Struder, Phys. Rev. A **68**, 013814 (2003).
[23] E. Constant, D. Garzella, P. Breger, E. Mevel, C. Dorrer, C. Le Blanc, F. Salin, and P. Agostini, Phys. Rev. Lett. **82**, 1668 (1999).
[24] T. Ruchon *et al.*, New J. Phys. **10**, 025027 (2008).
[25] M. B. Gaarde, M. Murakami, and R. Kienberger, Phys. Rev. A **74**, 053401 (2006).
[26] Y. Tamaki *et al.*, Phys. Rev. Lett. **82**, 1422 (1999).
[27] E. Brunetti, R. Issac, and D. A. Jaroszynski, Phys. Rev. A **77**, 023422 (2008).
[28] H. Xu, H. Xiong, Z. Zeng, Y. Fu, J. Yao, R. Li, Y. Cheng, and Z. Xu, Phys. Rev. A **78**, 033841 (2008).
[29] K. Varjú *et al.*, Laser Phys. **15**, 888 (2005).
[30] A. Zair *et al.*, Phys. Rev. Lett. **100**, 143902 (2008).